Original Research Article

GREENHOUSE GASES SCIENCE AND TECHNOLOGY

Visual investigation of CO_2 dissolution and convection in heterogeneous porous media at reservoir temperature and pressure conditions

Widuramina Sameendranath Amarasinghe and Ingebret Fjelde, NORCE Norwegian Research Centre AS, Stavanger, Norway and University of Stavanger, Stavanger, Norway
Anna Maija Nørstebø Flaata, University of Stavanger, Stavanger, Norway

Abstract: CO_2 convective mixing in saline aquifers has been widely studied numerically and experimentally. Reservoir heterogeneity is significant for CO_2 convective mixing and experimental studies are still limited. In this study, we have conducted a visualization of CO_2 convective mixing experiments in heterogeneous porous media at reservoir conditions using CO_2 and water. We have used a two-dimension Hele–Shaw cell, different glass beads of different permeability at porous media, and water solution with pH indicator. Glass beads were packed in a different way (horizontally and vertically) to generate the heterogeneity inside the test cell. We have studied transport velocity deviation due to the heterogeneity and effects of permeability transition zone together with the effects of boundary conditions. It was found out that having a low permeable layer below a high permeable layer restructure the flow of CO_2 fingers and dampens the CO_2 transport velocity. With the vertical permeability zones, having a high permeability zone accelerates CO_2 gravity transport through that zone which is a good representation for a fracture or a fault in the reservoir. CO_2 convection onset is governed by the vertical high-permeable layer. Boundary conditions have been dominant with the presence of high permeable zones. It also found out that the experimental results presented in this study match with the simulation studies that are available in the literature. © 2021 The Authors. *Greenhouse Gases: Science and Technology* published by Society of Chemical Industry and John Wiley & Sons Ltd.

Keywords: CO_2 density-driven convection; Hele–Shaw cell; heterogeneity; porous media; visualization

Introduction

The excessive Green House Gas (GHG) emissions cause a rise in Earth's temperatures. The process is known as global warming and already have made a highly injurious impact on life on Earth[1]. To alleviate global warming, there is a broad consensus that a significant reduction in atmospheric GHG concentrations must occur. This can be achieved by drastically reducing GHG emissions over the next few decades through carbon, capture, and storage (CCS).[1–3] As evaluations of CCS initiated it was suggested to implement geological CO_2 storage by injection into hydrocarbon reservoirs and deep saline

Correspondence to: Widuramina Sameendranath Amarasinghe, NORCE Norwegian Research Centre AS, Stavanger 4021, Norway
E-mail: widuramina@norceresearch.no
Received August 10, 2020; revised January 18, 2021; accepted February 11, 2021
Published online at Wiley Online Library (wileyonlinelibrary.com). DOI: 10.1002/ghg.2055

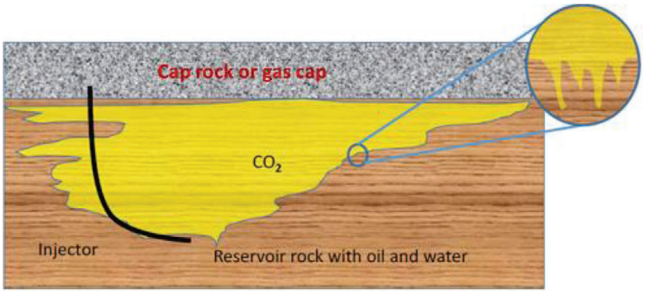

Figure 1. Simplified sketch of convection-driving dissolution of CO_2 with oil inside the reservoir.

aquifers. Thus, notwithstanding that deep aquifers are believed to have the largest storage capacity and be much more widespread than the other options.[1,4–7]

After CO_2 injection into the reservoir, CO_2 will be trapped by four mechanisms which can be identified as structural trapping, residual trapping, mineral trapping, and solubility trapping. Solubility trapping is one of the significant mechanisms for long term CO_2 storage.[8,9] At reservoir conditions (pressure and temperature), injected liquid or supercritical CO_2 (sCO_2) will have a lower density than the presence of the fluid. Hence CO_2 creates a plume under the caprock. Then CO_2 from this plume will mix with water below under the mechanism of solubility trapping (see Fig. 1). The CO_2 dissolution into the water-phase initiated by the diffusion, will increase the density of this phase and thereby accelerate the convective flow of CO_2. This process will contribute to CO_2 storage by accelerating the gravity-driven CO_2 dissolution.[10]

The convection-driven dissolution has been extensively studied experimentally for accelerated CO_2 dissolution in saline water under gravity for CO_2 storage inside two-dimension (2-dim) Hele–Shaw cells or 3-dimension (3-dim) cylindrical cells.[11–22] To make the CO_2 convective flow inside fluids (water or oil) analogous to 2-dim, Hele–Shaw cells are used.[23] Hele–Shaw cells are constructed by two parallel flat plates with a small gap in between (generally less than 10 mm). The thickness of the cell should be enough to allow a clear visualization. Vosper *et al.*[11] and Mahmoodpour *et al.*[12] have conducted CO_2 convective dissolution into water-saturated porous media using a 2-dim Hele–Shaw cell under gas conditions. Amarasinghe *et al.*[21] have conducted their experiments inside a Hele–Shaw cell at supercritical conditions (100 bar, 50 °C) where CO_2 was dissolved into water-saturated homogeneous porous media. A detailed review of the available CO_2 convective mixing experiments can be found at Amarasinghe *et al.*[21]

Most reservoirs are far from homogeneous.[24] They exhibit a complex structure and significant variations in the sizes and the packing of the rock grains, presence of impurities, the existence of fractures and faults.[25] This results in spatial variations of important reservoir properties, such as porosity and permeability, which are often associated with the heterogeneity of porous media. Spatial variations in any reservoir property can affect flow efficiency, but spatial variations in permeability, which can vary by several orders of magnitude, appear to have a particularly great influence.[26] Hence, reservoir heterogeneity can have a significant impact on density-driven convective mixing of CO_2.

CO_2 mixing in water/brine visualization experiments involving heterogeneity is very limited. Taheri *et al.*[14] have conducted a series of experiments of density-driven natural convection of CO_2 in saline water in a heterogeneous system. They have used a Hele–Shaw (50 cm × 50 cm × 12 mm) cell at atmospheric conditions (1 bar, 23 °C) for visualization investigations. Added different barriers inside the Hele–Shaw cell have been used to generate the heterogeneity. They have investigated the CO_2 finger behaviour with four different arrangements and each case has been discussed. According to their studies, each horizontal barrier had disturbed the CO_2 gravity movement and speeds vary depends on the vertical permeability and barrier properties.

Agartan *et al.*[27] have conducted an experimental study to investigate the contribution of heterogeneous semi-confining low-permeable shale layers for CO_2 dissolution in saline aquifers. They have conducted their study in an intermediate scale 3-dim laboratory apparatus using mimic fluids in sand packs. It was highlighted in their study the importance of considering deviations from the traditional mixing of CO_2 homogeneous porous media due to the reverse convection and trapping of CO_2 through diffusion. Wang *et al.*[28,29] have conducted CO_2 density-driven convection experiments using mimic fluids in a porous medium with homogeneous and heterogeneous layered structures using MRI technology. They have found out that when fingers go through the interface of heterogeneous layers with increased permeability, the finger velocity increases while the diameter of fingers

decreases vice versa when CO_2 pass through layers with decreasing permeability. Several other authors also have conducted the effects of heterogeneity for CO_2 convection[30–33] and trapping[34–36] in water using different mimic fluids and different type of porous medium.

But none of these studies has been conducted using actual sCO_2 and the presence of porous media. Hence it is important to have a set of experimental results using the actual fluids (sCO_2 and water) and actual reservoir conditions (pressure and temperature) to confirm the existing results and further development of the mathematical models.

Elenius *et al.*[37] have conducted a simulation study to investigate CO_2 convective mixing in formations with horizontal barriers. They have found out that the mass flux into the system is inversely proportional to the barrier length and proportional to the horizontal and vertical space of the barriers. Lin *et al.*[38] have conducted a simulation study of natural convection of dissolved CO_2 in small-scale heterogeneous saline formation. In their study, they have focused on the effects of small-scale permeability variations to the dissolved CO_2 in water. They have concluded that local permeability variations could trigger CO_2 fingering hence it will enhance the vertical CO_2 convection. Further numerical and simulations analysis has been carried out to investigate convective-diffusive CO_2 mixing in heterogeneous aquifers by several authors.[32,39–48]

In this paper, we have carried out a visual investigation of CO_2 convective dissolution into water-saturated heterogeneous porous media. A high-pressure 2-dim Hele–Shaw cell has been used for visual investigations. The results will be important in identifying of field-scale impacts and assessment of reservoir conditions for deep saline aquifers while simultaneously increasing the long-term CO_2 storage potential. To best of our knowledge, this is the first time CO_2 dissolution in water-saturated porous media experiments has been carried out at reservoir conditions.

Materials and methods

Experimental setup

The high-pressure 2-dim-cell was developed using stainless duplex steel and borosilicate glass. The 2-dim cell was designed for maximum working conditions of 150 bars and 100 °C. The test cell consists of several units, which are assembled to construct the final cell. The cell volume was formed by two glass plates separated by an adjustable spacer. The front view of the real cell with insulation is shown in Fig. 2(a). A 3-dim sketch of the cell is shown in Fig. 2(b) while a cross-section of the cell is shown in Fig. 3. A specially designed filter module of shaped glass filter (pore size of 10–16 μm) plate was placed at the inlet and outlet to avoid penetrating the glass beads away from the test volume (see Figs. 2(b) and 3). The location of the gas injection was placed in the middle of the top filter module unit as shown in Fig. 3. The diameter of the test volume is 200 mm while the sight disk glass diameter was 100 mm. The thickness is 5.0 mm. Amarasinghe *et al.*[21] have provided further details of the high-pressure 2-dim cell and its design specifications.

Materials

Aqueous 0.04 wt% bromothymol blue (BTB) pH indicator solution (deionized water mixed with 0.01 M NaOH and BTB) of pH around 8.6 was used as the water phase. The BTB pH indicator is blue above pH 7.6 and yellow below pH 6.5, and green between these pH-values.[49] When CO_2 is dissolved in water, the pH will be reduced due to the release of H^+ ions, which will lead to the colour change in the water phase from blue to yellow.[50] Hydrophilic glass beads of different diameters were used to prepare porous media of different permeabilities (0.5, 16, 52, and 76 D). The permeability of the bead packs was determined by the waterflooding of tubes. The cumulative particle size distribution is shown in Fig. 4. The reason to select given permeabilities for the experiments was to avoid penetrating small particles in the lower permeable beads layer into the high permeable beads layer during the packing and during the experiment.

Experimental procedure

The experimental set-up with the high-pressure 2-dim test cell is shown in the piping and instrumentation diagram (P & ID) (see Fig. 6). A back-pressure regulator was included in the set-up to avoid sudden developments of high-pressures inside the cell. CO_2 was introduced from a piston cell. A digital manometer was connected directly to the 2-dim cell for accurate reading of the absolute pressure.

Greenhouse Gas Sci Technol. **11**:342–359 (2021); DOI: 10.1002/ghg.2055

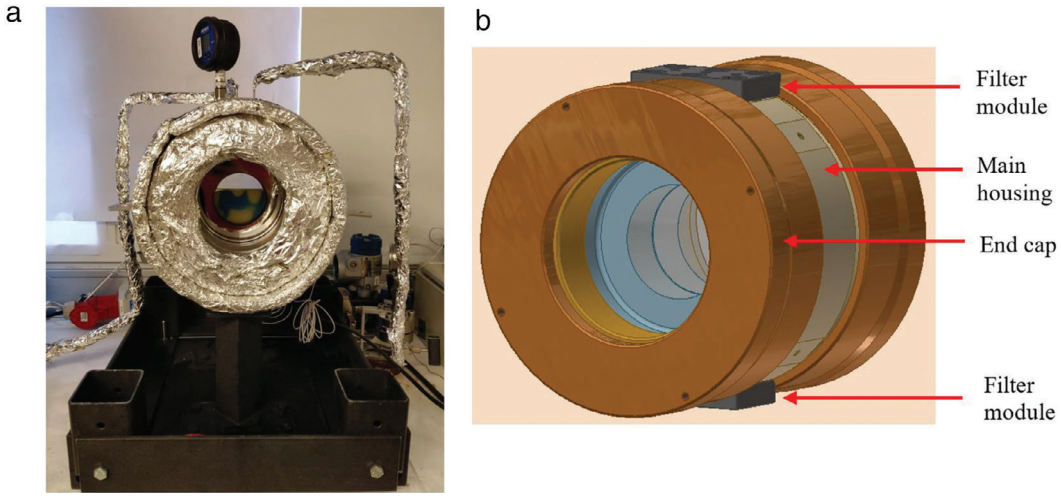

Figure 2. (a) Front view of the actual experiment setup. (b) 3-dim sketch of the high-pressure cell including main components.

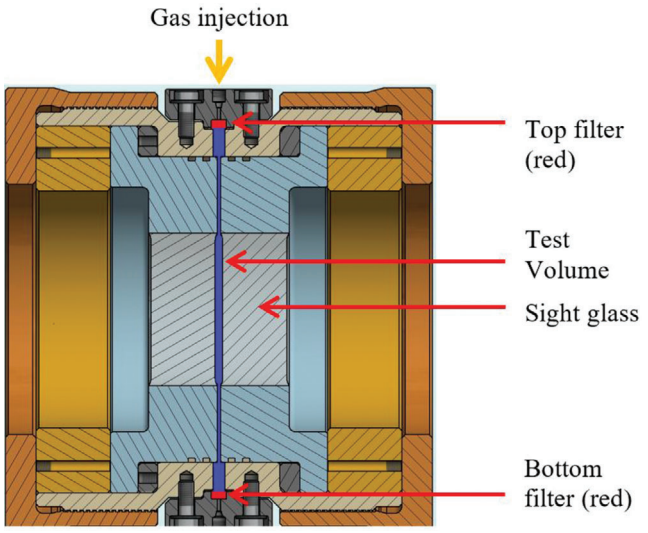

Figure 3. Cross-section of the high-pressure cell highlighting the test volume, filter locations, and gas injection location.

All the experiments were carried out at 50 °C and 100 bars. Glass beads were packed accordingly with horizontal layers or vertical layers as described below.

1. Beads packing with horizontal layering: Water solution was added into the 2-dim cell. Then one set of dry glass beads was filled manually from the top of the cell gradually so that the beads will settle smoothly inside the oil phase. When the desired level of porous media was achieved with the size of the particular beads, small external vibration was applied to the cell by using a plastic hammer to further settle the glass beads. Then the next set of beads was filled top of the previous layer and followed by the same procedure until all the required glass beads layers were filled and packed accordingly. See Fig. 8 at $t = 3$ mins for a final packed bead with horizontal layers.
2. Beads packing with vertical layering: Flexible plastic straws (at room temperature) were inserted into the 2-dim cell from the top. The straw's diameter was 8 mm whereas the space between sight disks was 5 mm, which made a vertical barrier for beads inside the 2-dim cell. The water solution was added into the 2-dim cell. Then one set of glass beads was filled into the middle part and then another set into the sides. The highest permeability beads were filled first regardless of the location to avoid small bead penetration into the next layer. When the beads are settled, straws were slowly taken out from the top. Beads were re-arranged slightly along the boundaries to occupy the space which was earlier occupied by the straws. Detail images of the vertical packing process are demonstrated in Fig. 5.

Finally, the 2-dim test cell was heated up to 50 °C.

After placing the filter module on the top of the cell, the cell was left for approximately half an hour to stabilize the temperature (confirmed from a thermal image by a FLUKE®, Fluke Corporation, USA, Ti25 thermal imaging camera).

The CO_2 piston cell was first filled to 80 bars at room temperature and then heated to 50 °C. After the gas

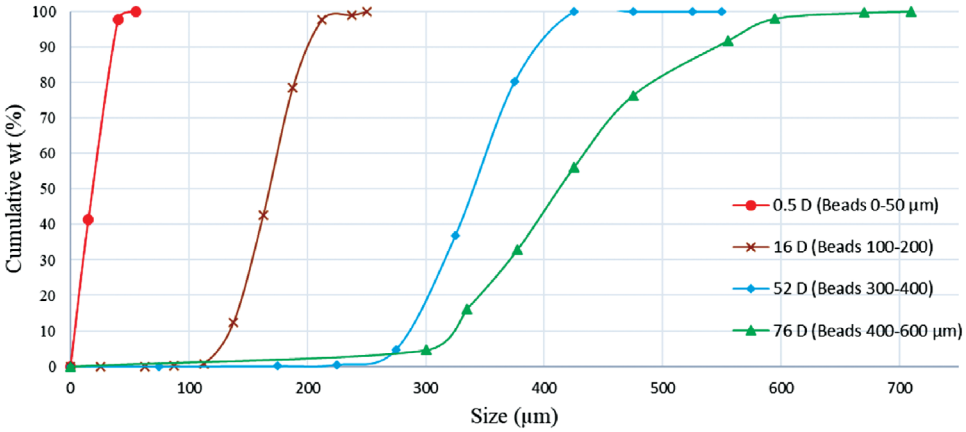

Figure 4. Cumulative particle size distribution of the glass beads.

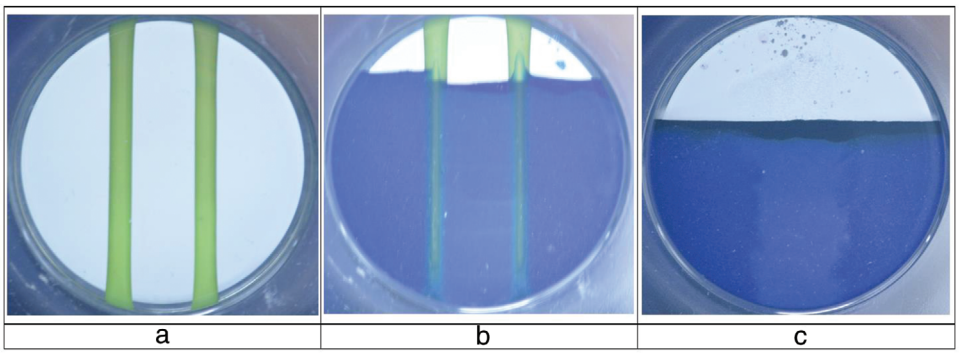

Figure 5. Step by step filling procedure for vertically layered alternating permeability porous media using straws. (a) Empty 2-dim cell with straws in (b) Beads packed into three vertical layers with alternating permeability (c) Final packing after straws have been taken out.

expansion, the piston cell was pressurized to 105 bars. The fine valve connected to the CO_2 piston cell (see Fig. 6), was then opened slowly to allow CO_2 flow into the 2-dim cell to avoid the splash of CO_2 into the liquid phase and movement of glass beads.

The visualization observations were carried out a Nikon D5200 camera with video interval image recording. There is a colour difference in each porous media layer due to the difference in glass beads sizes which leads to different light penetration/ retroreflection as seen in 'C' in Fig. 7 and $t = 3$ min in Fig. 8.[51]

Image analysing method

ImageJ open-source image analysis software[52] was used to analyse the transport velocities of the CO_2 front. Longest CO_2 finger length or location of the CO_2 front in each section/layer was used to calculate the CO_2 transport velocity within that section.

Experimental cases

Horizontal layering and vertical layering experiment that has been carried out in this study are provided in Tables 2 and 3, respectively. Figure 7(a) and (b) provide the guide for the data given in Tables 2 and 3, respectively.

Rayleigh number (*Ra*) calculation

Rayleigh number (Ra) was calculated using the equation; $Ra = (\Delta\rho g k H)/(\mu D \Phi)$ where $\Delta\rho$ is the density increase of water due to CO_2 dissolution, g is the acceleration of gravity, k is the permeability of the porous media, H is the height of porous media, μ is the dynamic viscosity of the oil, D is the molecular diffusion coefficient of CO_2 in oil and "Φ" is the porosity of porous media. Parameter values used to calculate the Ra number are given in Table 1. Ra number which is a dimensionless number of the ratio between free convection to diffusion, should be equal

Greenhouse Gas Sci Technol. **11**:342–359 (2021); DOI: 10.1002/ghg.2055

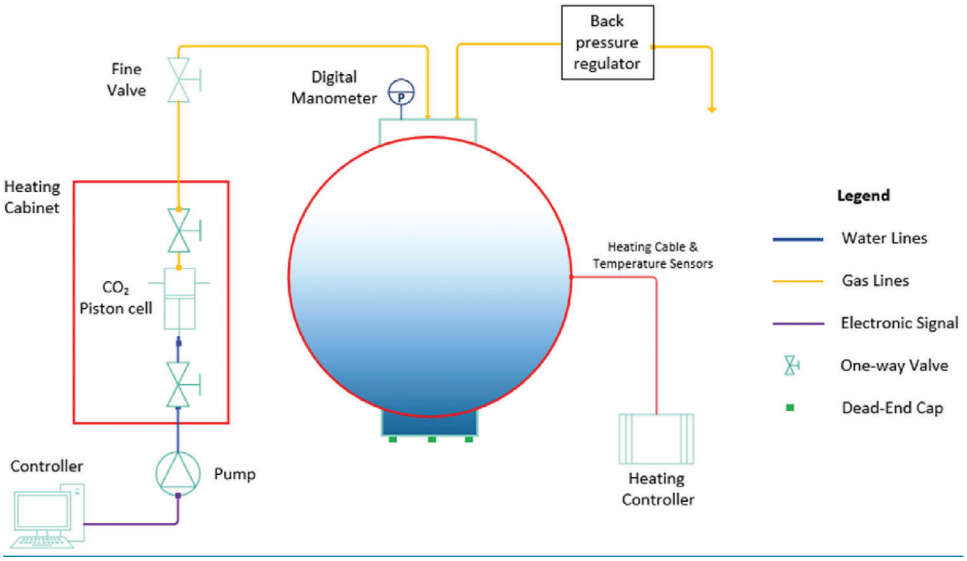

Figure 6. Piping and instrumentation (P & ID) diagram of the experimental setup.

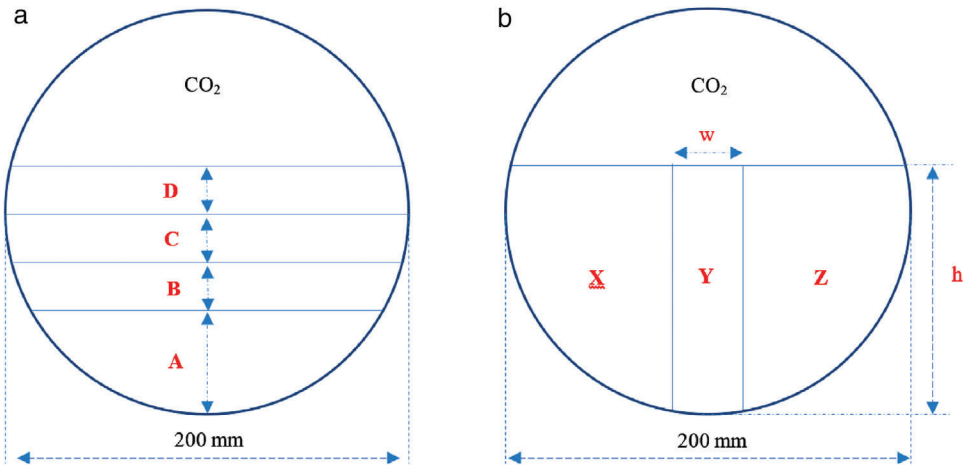

Figure 7. Sketch of the packing of the (a) horizontal layers and (b) vertical layers.

Table 1. Parameters for Ra number calculation.

Parameter	Value**	Units
ρ_{CO_2}	384.67	kg m^{-3}
ρ_{water}	988.05	kg m^{-3}
$\rho_{(water+CO_2)mix}$ [58,59]	1002.8	kg m^{-3}
$\Delta\rho$	14.75	kg m^{-3}
D[60]	$3.643*10^{-9}$	m^2 s^{-1}
μ	5.474×10^{-4}	kg/s·m

**Obtained at 50 °C/100 bar.

or greater than $Ra_{critical}$, $4\pi^2$ (39.47), for the natural convection to become substantial.[17,53] *Ra* number for the layers in each experimental case are also presented in Tables 2 and 3.

Results and discussion

As given in Tables 2 and 3, visualization experimental results of CO_2 transport inside heterogeneous porous media are presented below.

Horizontal layering

Figures 8–11 shows experimental visualization results from cases 1–4, respectively. Cases 5 and 6 visual images are not presented due to the similarities with case 1. The CO_2 front development of cases 1, 2, and 3 are shown in Figs. 12, 13, and 14, respectively. The CO_2 front development of cases 5 and 6 is presented in Fig. 15. The height of the longest finger/CO_2 front was considered for the CO_2 front development

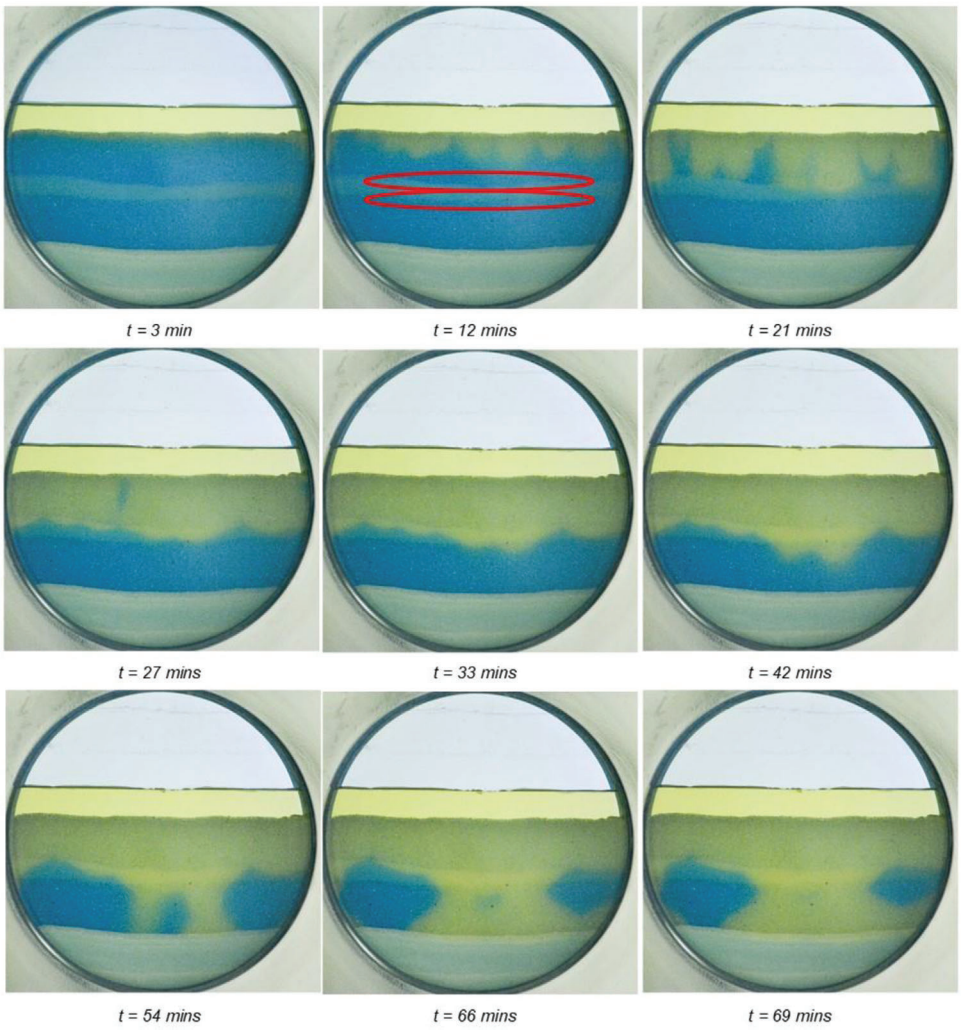

Figure 8. Experimental snaps from case 1 with horizontal layering (0.5, 76, 16, 76 from bottom to upwards) showing CO_2 front movement.

measurements. The CO_2 linear transport velocity is also presented for each permeable layer in Figs. 12–15.

In case 1, as shown in Fig. 8, CO_2 fingering was first observed in the high permeable layer (76 D) which was placed at the top. When CO_2 reached the low permeable layer of 16 D (second layer), CO_2 flattened out along the low permeable layer as shown at $t = 21$ min in Fig. 8. CO_2 fingers merged in the top high permeable layer while CO_2 was transporting through the 16 D permeable layer. The CO_2 transport velocity dampened significantly as it can be seen in Fig. 12, where the CO_2 front length gradient reduces. When CO_2 reached the third bottom layer of 76 D again, CO_2 fingering was observed, but in a reduced number of fingers (see $t = 42$ min in Fig. 8) because the onset of CO_2 has been disturbed by the low permeable layer from the top. Again, when CO_2 reached the fourth layer of 0.5 D, CO_2 was dampened along with the beads layer. The trends were similar in cases 5 and 6 where 52 D beads were used instead of 76 D. In case 6 a higher height of lower permeable beads (16 D) layer was used compared to case 5 to observe the dampened effect due to the height of the low permeability layer as seen in Fig. 15.

In case 2, the opposite arrangement of permeability layers was arranged where a high permeable layer (76 D) was placed in the middle while having two low permeable layers (16 D) on top and bottom. Hence, in the beginning, the CO_2 front was moving slowly in the low permeable porous media and then accelerated in the high permeable layer and again dampened in the low permeable layer (see Fig. 13). Compared to case 1

Greenhouse Gas Sci Technol. **11**:342–359 (2021); DOI: 10.1002/ghg.2055

Table 2. Set of horizontal layering experiments.

		Horizontal layers as in Figure 7(a)				
Case #	Parameter	A	B	C	D	Results
Case 1	Permeability (D)	0.5	76	16	76	Figures 8 and 12
	Height—H (mm)	23.8	16.1	5.3	18.1	
	Ra number	2.1	219.1	15.2	246.3	
Case 2	Permeability (D)	0.5	16	76	16	Figures 9 and 13
	Height—H (mm)	21.1	15.2	7.6	16.4	
	Ra number	1.9	43.5	103.4	47	
Case 3	Permeability (D)	0.5	16	52	76	Figures 10 and 14
	Height—H (mm)	30.9	15.5	17	18.2	
	Ra number	2.8	44.4	158.3	247.6	
Case 4	Permeability (D)	0.5	16	52	16	Figure 11
	Height—H (mm)	25.1	17.1	21	17.1	
	Ra number	2.2	49	195.5	49	
Case 5	Permeability (D)	0.5	52	16	52	Figure 15
	Height—H (mm)	26.9	22.6	4.8	15.3	
	Ra number	2.4	210.4	13.7	142.4	
Case 6	Permeability (D)	0.5	52	16	52	
	Height—H (mm)	20	29.2	13	17	
	Ra number	1.8	271.8	37.2	158.3	

Table 3. Set of vertical layering experiments.

		Vertical layers as in Fig. 7(b)			Width of the centre vertical layer, w (mm)	The total height of the packing, h (mm)	Results
Case #	Parameter	X	Y	Z			
Case 7	Permeability (D)	16	76	16	26	62	Figure 17
	Ra number	177.6	843.6	177.6			
Case 8	Permeability (D)	76	16	76	28	56.2	Figure 18
	Ra number	764.7	161	764.7			

top layer (76 D with a *Ra* number 246.3) a smaller number of fingers were observed in case 2 top layer (16 D with a *Ra* number of 47). Due to lower *Ra* number of the top layer in case 2, CO_2 has lesser convective-driven flux compared to case 1 top layer.[21] A similar permeability layer arrangement was carried out in case 4, but instead of 76 D porous medium 52 D porous medium was selected (see Fig. 11). But in this case, it was observed that CO_2 transport was getting a high disturbance due to the boundary effects. Hence, the CO_2 front development of case 4 was not calculated.

In case 3, horizontal layers were arranged in descending order of permeability from top to bottoms such as 76, 52, 16, and 0.5 D. The CO_2 transport was damping in a very smooth manner in this case due to the downgrading permeability as clearly seen in Fig. 14. The number of fingers was reducing in each layer as seen in Fig. 9 and as usual, fingers were damping along with the layers. It was observed that when the top layer permeability is lower compared to the second layer permeability, boundary effects became dominant in the higher permeable layer as seen in Fig. 11.

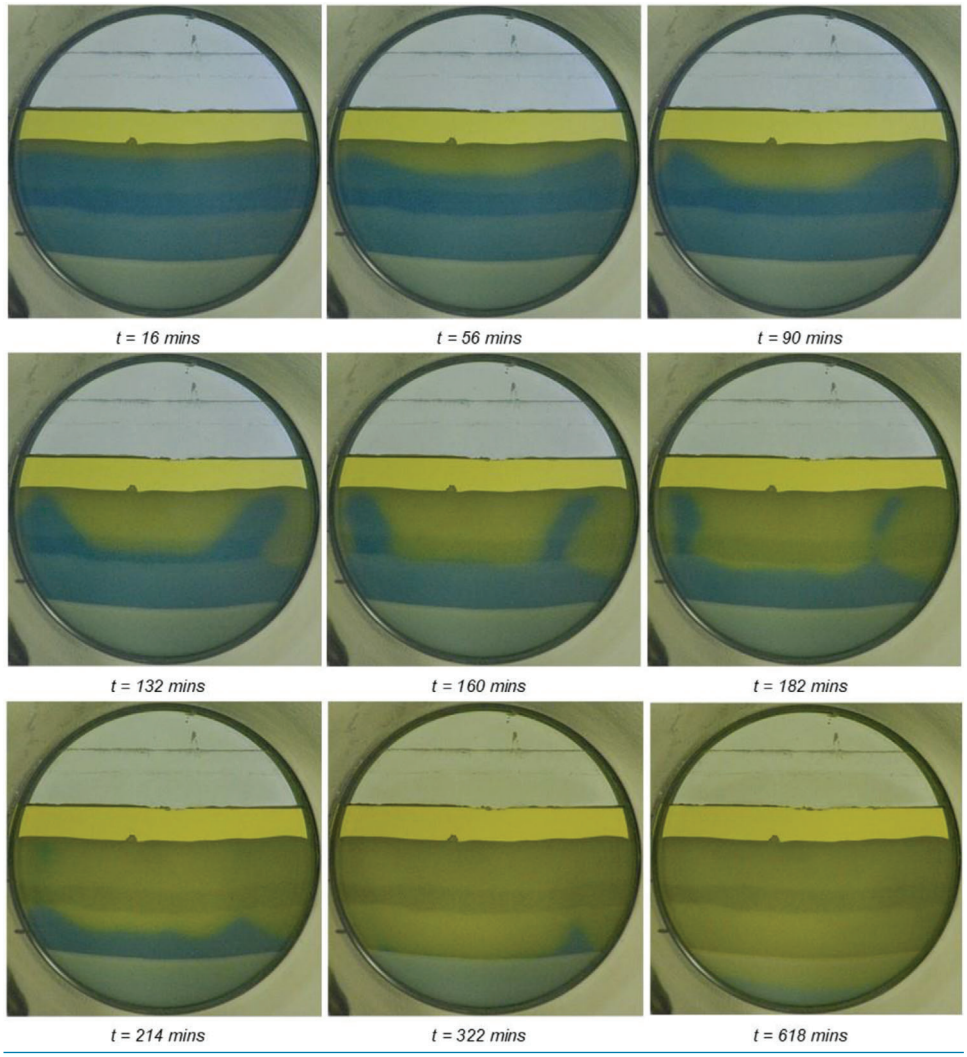

Figure 9. Experimental snaps from case 2 with horizontal layering (0.5, 16, 76, 16 from bottom to upwards) showing CO_2 front movement.

To have a better realistic and scaled analysis of the experimental results, *Ra* number was used. In Fig. 16 it is shown the relationship between *Ra* number versus CO_2 transport velocity for experimental cases with sandwich-like horizontal layering (case 1, 2, 3, and 4). CO_2 transport velocity inside the bottom layer with 0.5 D was neglected for the analysis mainly because CO_2 flux is affected by the boundary effects when reached to 0.5 D layer. When having the same permeability on top and bottom layers, CO_2 transport velocity inside the bottom layer have a lower value (see ∗data points in Fig. 16) compared to the top layer (see △ data points in Fig. 16). It is also noticed that *Ra* number for the middle layer of 16 D in cases 1, 5, and 6 is lower than the critical value. As seen in Fig. 8 at $t = 27$ min, CO_2 transport front become dampened in these middle layers which indicates a piston-like displacement with a diffusion dominant CO_2 flow. It was observed that in case 6, with top layer of 52 D (with *Ra* number of 158.3) velocity was higher compared to the case 1 where the top layer was with 76 D (with *Ra* number of 246.3). In case 6, middle layer (16 D) had a *Ra* number of 37.2 which is closer to critical value of 39.47. Meanwhile in case 1 had a *Ra* number of 15.2 in the middle layer. In comparison, it was alleged that, having a *Ra* number which is closer to convection dominance (i.e., closer to critical value) in the middle layer annulated the top layer CO_2 transport flux in case 6.

Vertical layering

Figure 17 shows the snaps from the experiment (case 7) with a high permeability layer (76 D) in the middle

Greenhouse Gas Sci Technol. **11**:342–359 (2021); DOI: 10.1002/ghg.2055

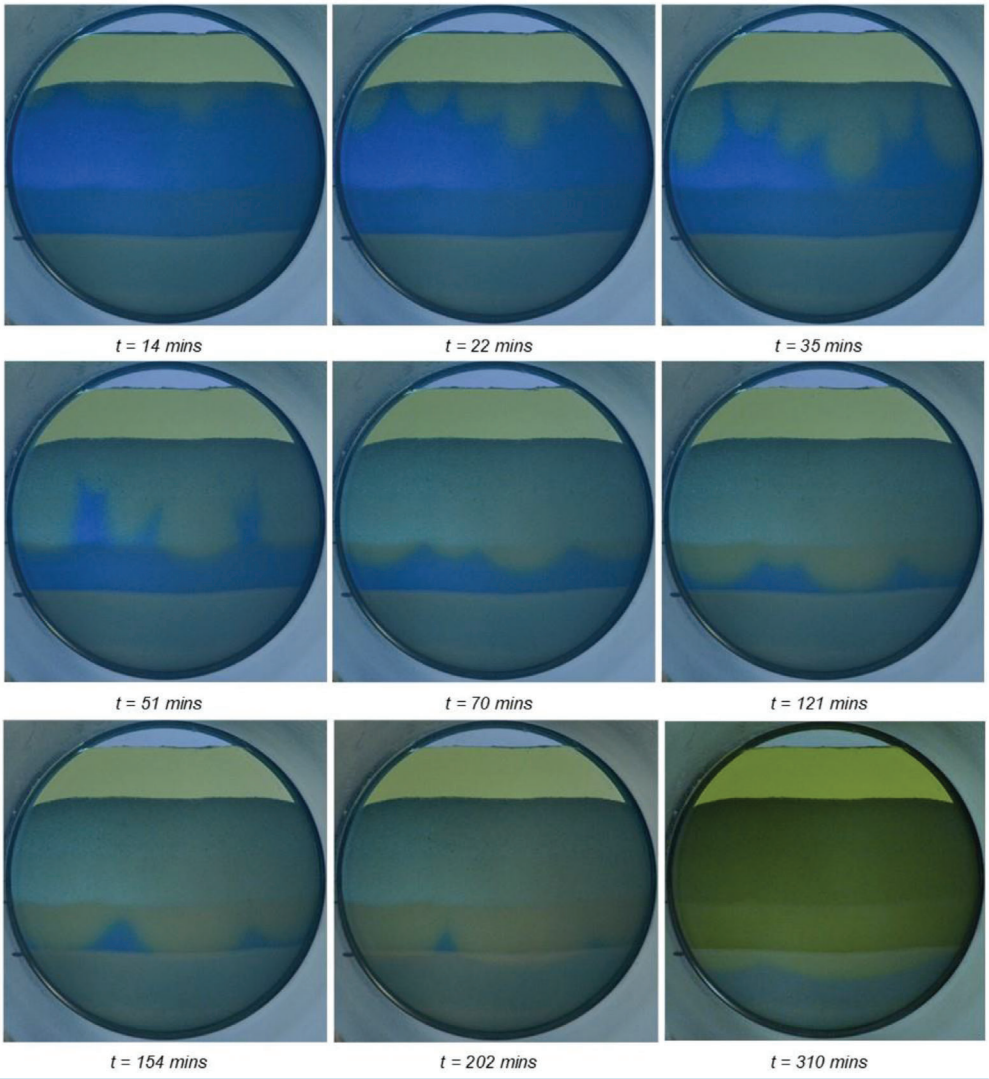

Figure 10. Experimental snaps from case 3 with horizontal layering (0.5, 16, 52 , 76 D from bottom to upwards) showing CO_2 front movement.

and low permeability layers (16 D) in the sides. This high-permeable layer can represent a vertical fracture of higher permeability or a fault in a reservoir. CO_2 mixing was initiated and was dominant in the high permeable layer. Several fingers were seen at the beginning of the experiment in the high-permeable layer in between two low-permeable layers (see from $t = 3$ min to $t = 11$ min in Fig. 17). With time the fingers merged though the high permeable layer. Meanwhile, in the low permeable layer CO_2 diffusion was observed (see circled area in Fig. 17 at $t = 9$ min). Due to the high permeability contrast, CO_2 though the middle layer reached the bottom of the cell, while CO_2 was transporting towards into the low permeable layers in sideways as seen from $t = 42$ min to $t = 155$ min in Fig. 17 (shown with red arrows).

Figure 18 shows the snaps from the opposite experiment of case 7 (case 8) where a low permeable layer was placed in the middle (16 D) while high permeable layers (76 D) were placed in the sides. In this case, fingers were formed in the high-permeable layers at each side, while the low-permeable layer in the centre of the cell was dominated by diffusion at the beginning. CO_2 transported through the high permeable layers migrated into the low permeable layer from the sides as seen from $t = 76$ min to $t = 135$ min in Fig. 18. It was also observed that CO_2 countered along with the boundary influenced for the CO_2 to

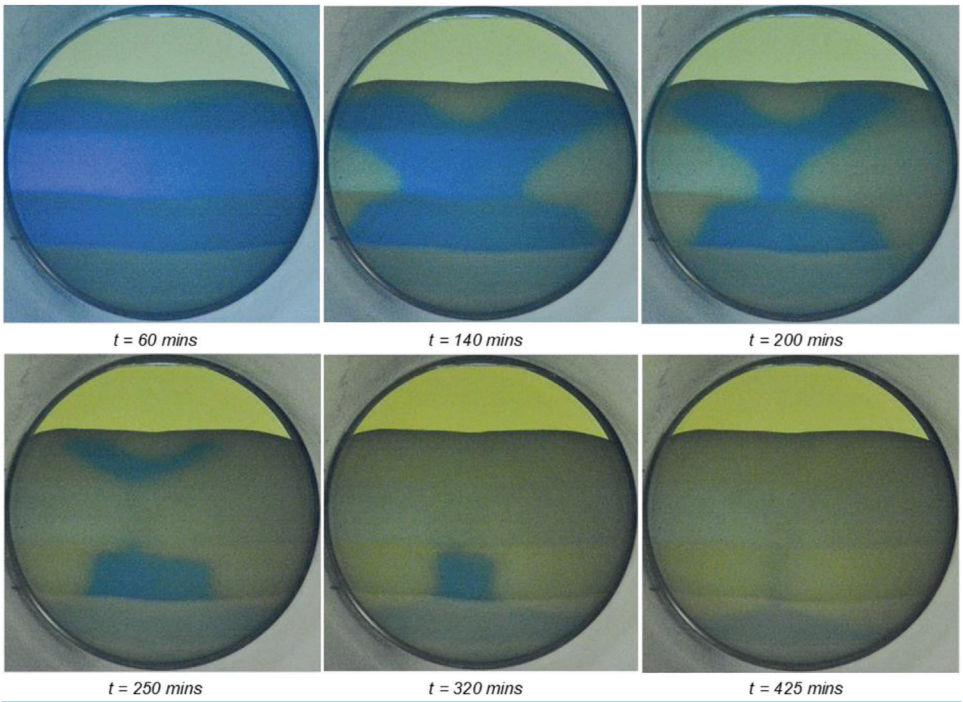

Figure 11. Experimental snaps from case 4 with horizontal layering (0.5, 16, 52, 16 D from bottom to upwards) showing CO_2 front movement.

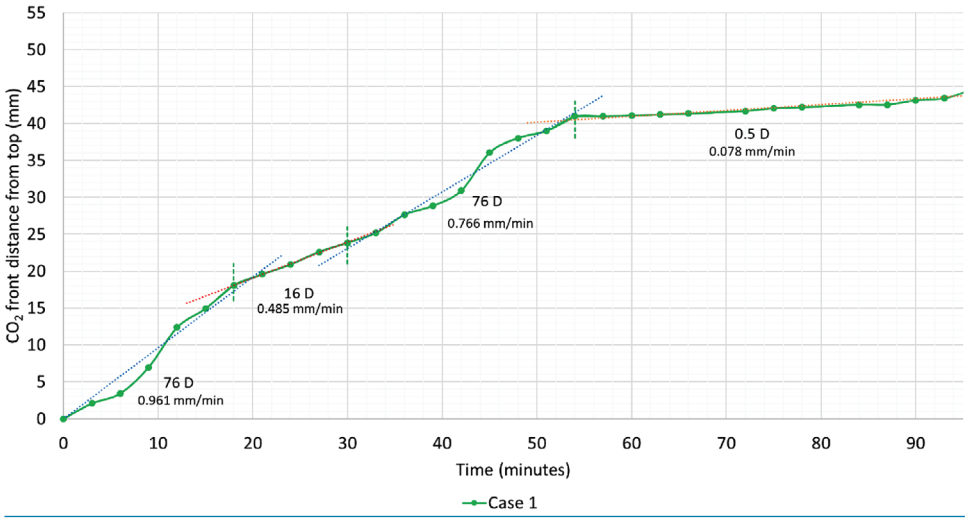

Figure 12. CO_2 front development for case 1 with linear transport velocity in each horizontal layer.

transport into the low permeable layer. Which is the reason for CO_2 transport into the low permeable layer from the bottom of the packing as shown in red arrows at $t = 76$ min in Fig. 18. In both cases 7 and 8, the rates of finger growth (1.8 mm min^{-1}) inside high permeability layer (76 D) were very similar to the rate of the reference experiment of 76 D permeability conducted by Amarasinghe *et al.*[21] with the same height of porous media pack (i.e., with closer *Ra* number).

General discussion

We have conducted the same experiments in low pressure (10 bar) and room temperature conditions and have observed a similar pattern in CO_2 transport. But due to low pressure, CO_2 transport through the

Greenhouse Gas Sci Technol. **11**:342–359 (2021); DOI: 10.1002/ghg.2055

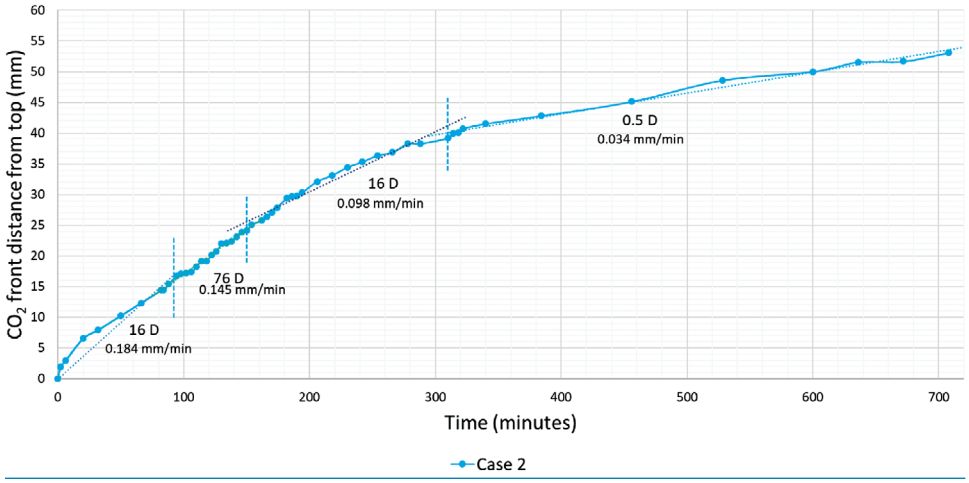

Figure 13. CO_2 front development for case 2 with linear transport velocity in each horizontal layer.

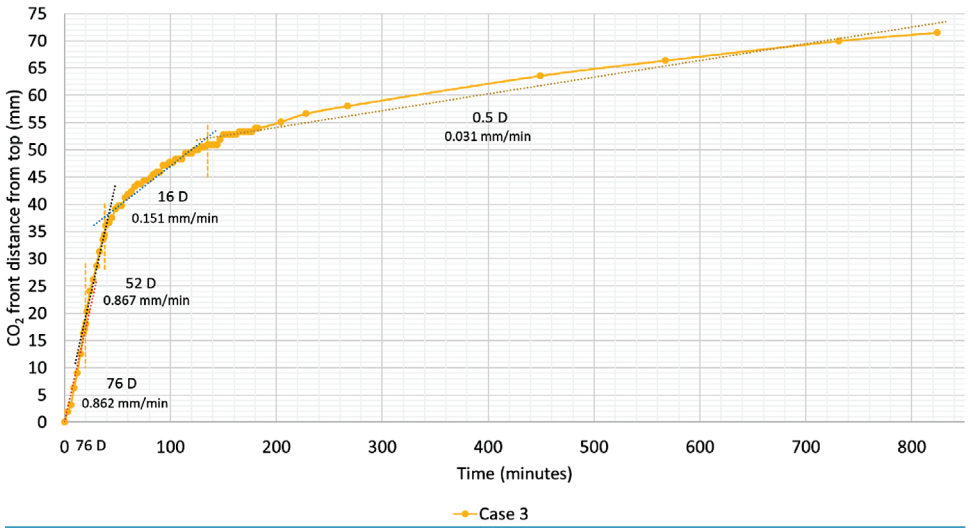

Figure 14. CO_2 front development for case 3 with linear transport velocity in each horizontal layer.

porous media has been slower compared to this present study hence boundary effects also have been dominant in some cases.[54] In heterogeneous permeability experiments, a horizontal low-permeable layer in between high-permeable layers attenuated the density-driven convection, while density-driven convection occurred in a vertical high-permeable layer rather than in the low-permeable layers surrounding it. The results also coincide with the results of simulations performed by Lin *et al.*[38] and Chen *et al.*[46] in which relatively high local permeability values just below the CO_2-water interface was found to trigger instabilities in the diffusive layer and influence the number of fingers developing initially. Also, their findings that the finger development was substantially controlled by the permeability below the fingers and along their paths match our experimental results. Similarly, Farajzadeh *et al.*[45] and Kim *et al.*[43] found through their simulations that finger development correlated strongly with the permeability distribution in cases with a moderate degree of heterogeneity, that is, fingers developed in the high permeability regions.

In vertical layering, CO_2 convection onset is governed by the vertical high-permeable layer. Due to the representation of reservoir conditions (i.e., crack or faults) in the presented vertical experiments, consequently, these experiments may be relevant to CO_2 storage in actual reservoirs. The results obtained

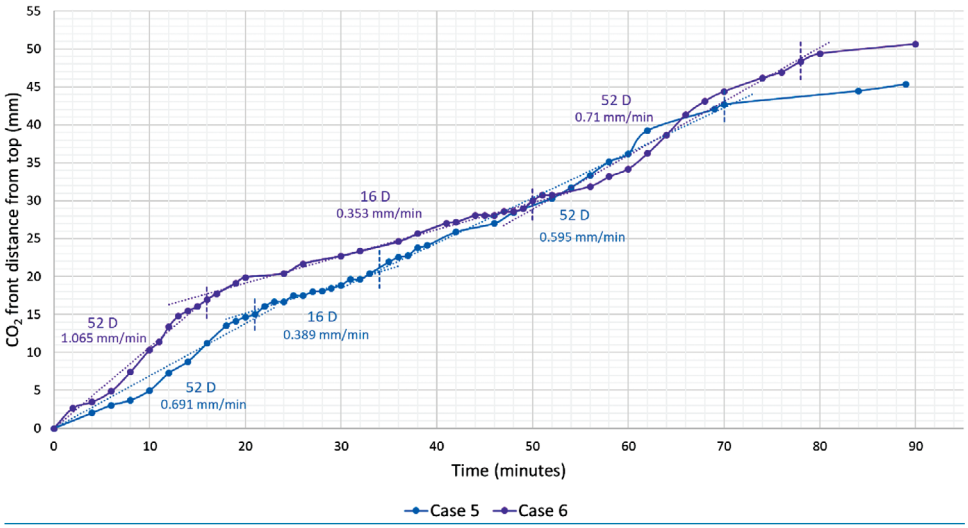

Figure 15. CO_2 front development for case 5 and 6 with linear transport velocity in each horizontal layer (values are provided in two different colours foreach case).

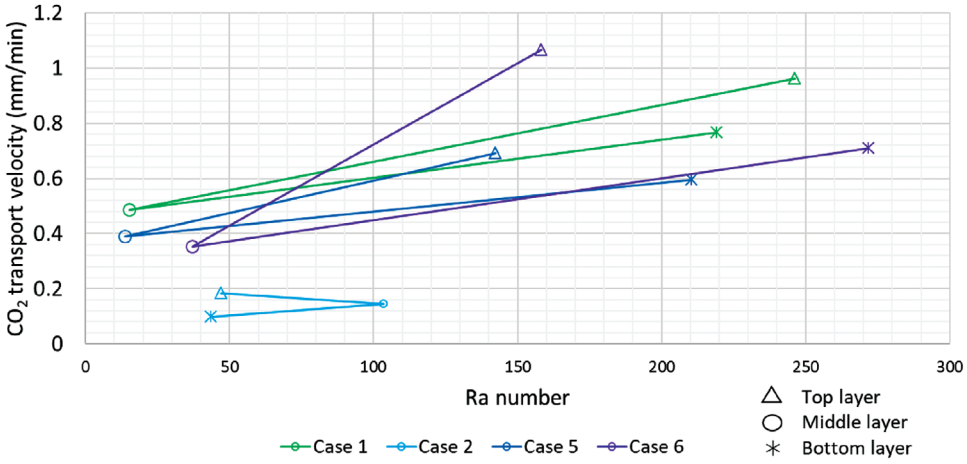

Figure 16. Ra number versus CO_2 transport velocity for experimental cases with sandwich like horizontal layering (case 1, 2, 3, 4). The data point for horizontal layers are presented as; top layer (△), middle layer (○), and bottom layer (∗).

from cases 7 and 8 coincide with the simulations that have been carried out by Chen *et al.*[40] and Rezk and Foroozesh[39], where they have simulated CO_2 density-driven convection with the presence of a fracture.

Limitations with packing

Since filling of the porous media into the cell was performed manually, obtaining a sharp interface between different types of permeability layers was problematic. Due to the particle size distribution, a transition zone between two layers was generated as shown in red circles in Figure 8 for horizontal layering and in Figure 17 for vertical layering. This transition layer affects the CO_2 transport velocity and convection since the permeability value of this zone lies in between two permeable values of the layers that surround it.

Usage of very high-permeable porous media

In this study, we have used glass beads ranging from 0.5 to 76 D in permeability. Reservoir permeability generally can vary between 1 mD and 10 D[55] with few exceptions like Johan Sverdrup.[56] The selected permeabilities such as 16, 52, and 76 D are far greater than realistic permeability values. In our previous study, we have observed that CO_2 density-driven convection does not occur with 0.5 and 4 D permeability.[21] Hence with the limitation of cell width,

Greenhouse Gas Sci Technol. **11**:342–359 (2021); DOI: 10.1002/ghg.2055

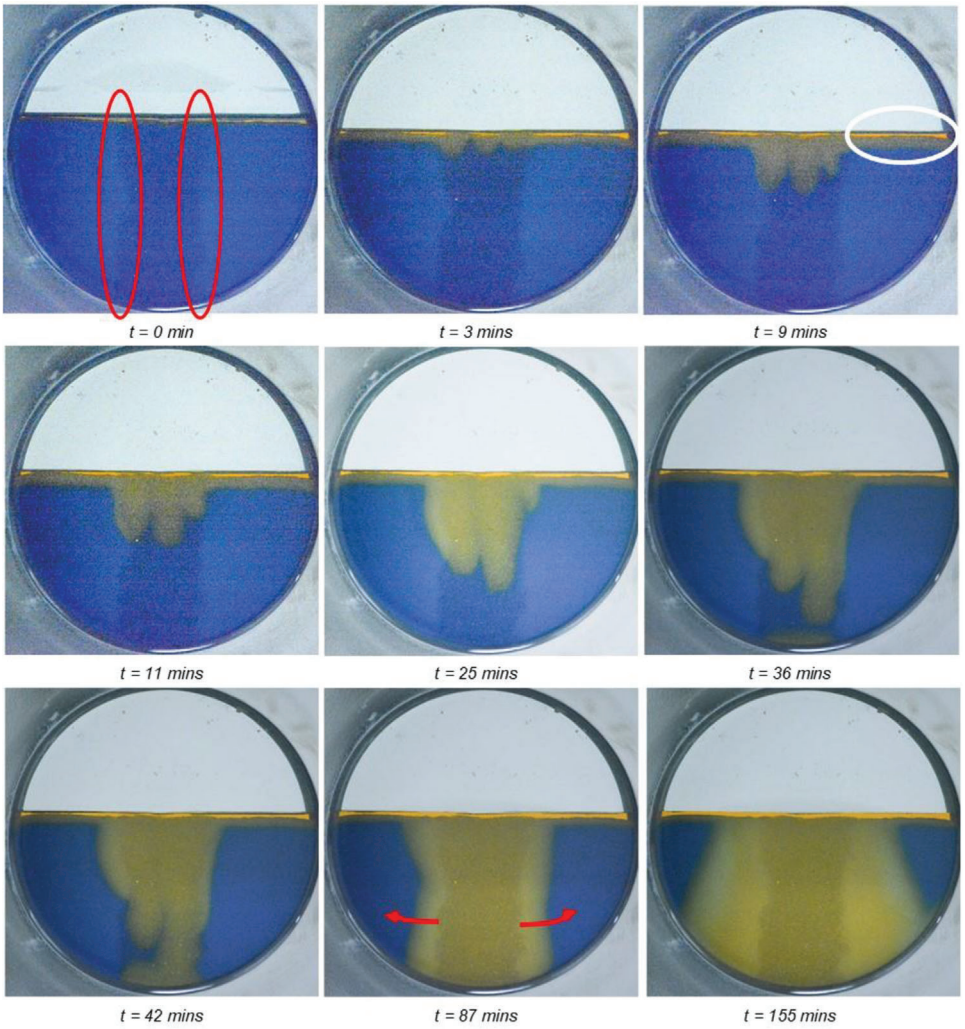

Figure 17. Experimental snaps from case 7 with vertical layering (16, 76, 16 D) showing CO_2 front movement.

we opted to use high permeable porous media to obtain CO_2 density-driven convection and fingering. Hence by observing CO_2 convective fingering within our cell dimension at higher permeabilities, the results can be used in scaling-up mathematical models to match with more realistic reservoir permeabilities.

Boundary effects

Due to the cell's circular geometry, if the cell was packed with a high-permeable porous medium, sometimes CO_2-saturated water appeared to flow faster along the curved edge of the cell. Consequently, when CO_2-saturated water from both the left and right sides reaches the bottom of the cell, it is forced to flow upwards through the porous medium (see Fig. 19). This counteracts the downward migration of CO_2-saturated water like in case 4 as shown in Fig. 11 where the boundary effects have been more dominant. The artifact invalidates some of the results as in cases 4 and 8. To limit the artifact to a minimum level a layer of 0.5 D porous media was packed in each experiment at the bottom, hence even though CO_2 saturated water flows along the boundary, the very low permeable layer at the bottom limits the flow upwards.

Difference between 2-dim experiments vs actual 3-dim reservoir

In the experiments, the CO_2 dissolved in the 5 mm spacing between two parallel sight disks, which provides a narrow, quasi-2-dim environment. The word 'quasi-2-dim' is used because the spacing between the sight discs causes some 3-dim effects.

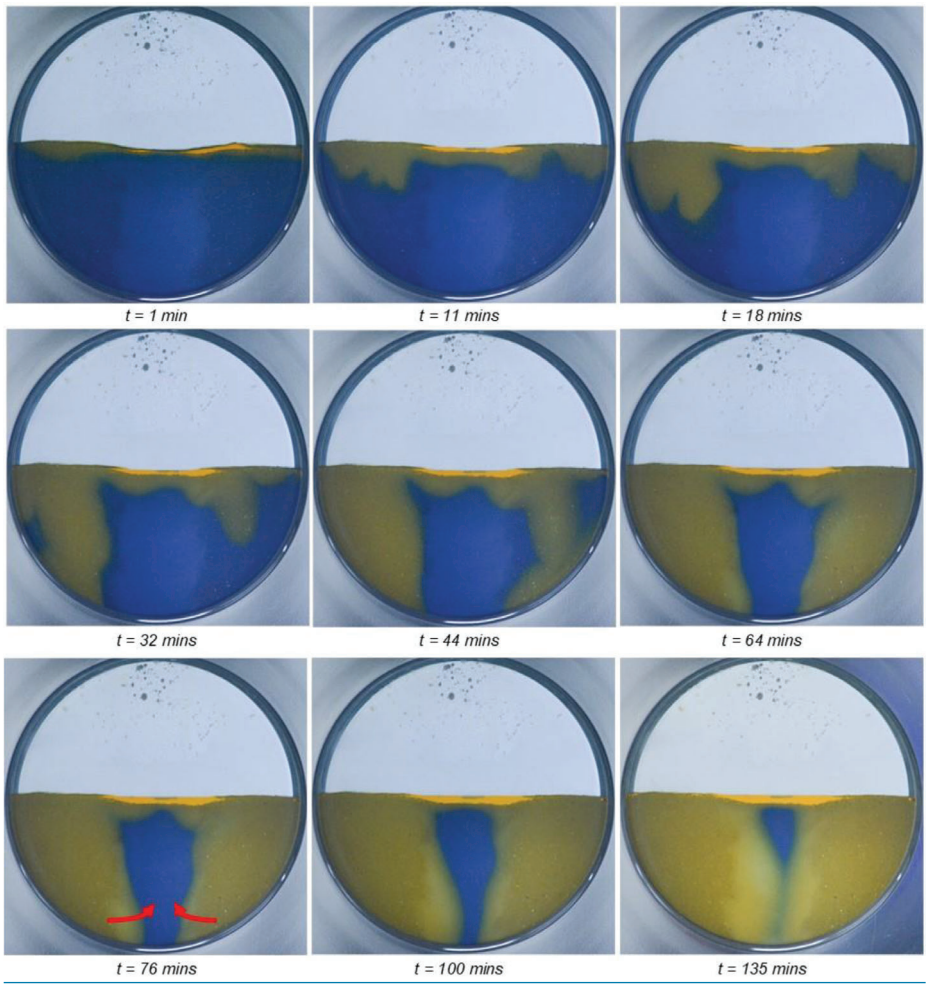

Figure 18. Experimental snaps from case 8 with vertical layering (76, 16, 76 D) showing CO_2 front movement.

However, neither 2-dim nor quasi-2-dim effects probably occur in an actual reservoir, which will be fully 3-dim in its flow nature. Despite this, Lindeberg *et al.*[57] stated in their simulation study that '*The timing of the onset of convective mixing is independent of whether one considers the problem in 2D or 3D*'. They also stated that the rate of convection most likely is slightly more efficient in a 3-dim than in a 2-dim environment, as there is more space for convective currents in 3-dim models. Consequently, by neglecting other differences between the cell and a real reservoir, one might expect the onset of convection to initiate at the same time in the 2-dim cells and 3-dim reservoirs.

Conclusions

To our knowledge, for the first time, we have conducted visualization of CO_2 convective mixing experiments in heterogeneous porous media at reservoir conditions using CO_2 and water. Differently packed (horizontally and vertically) glass beads with different permeability have given a good insight on how CO_2 convectively transport inside water-saturated heterogeneous porous media. We have studied transport velocity deviation due to the heterogeneity and effects of permeability transition zones. A horizontal low-permeable layer in between high-permeable layers attenuated the density-driven convection and restructured the flow of CO_2 fingers, while density-driven convection occurred in a vertical high-permeable layer rather than in the low-permeable layers surrounding it. With the vertical permeability zones, having a high permeability zone accelerates CO_2 gravity transport through that zone which is a good representation for a fracture or a fault in the reservoir. CO_2 convection onset is governed by the vertical

Greenhouse Gas Sci Technol. **11**:342–359 (2021); DOI: 10.1002/ghg.2055

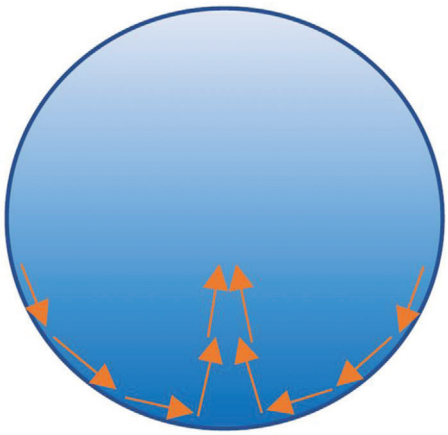

Figure 19. Illustration of boundary effects artefacts due to the cell geometry.

high-permeable layer. Boundary conditions have been dominant with the presence of high permeable zones. It also found out that the experimental results presented in this study match with the simulation studies that are available in the literature.

Funding

Research Council of Norway — CLIMIT program.

Conflict of Interest

The authors declare that they have no conflict of interest.

Acknowledgements

The authors would like to thank the Research Council of Norway for the funding of this research project through the CLIMIT program which is dedicated to the accelerating and the commercialization of Carbon Capture and Storage (CCS) through research, development, and demonstration. Also, the Authors would like to mention Jan-Åge Rydland for the support with the design and the construction of the experimental setup.

References

1. IPCC. *IPCC Special Report on Carbon Dioxide Capture and Storage*. Prepared by Working Group III of the Intergovernmental Panel on Climate Change Cambridge, UK and New York; (2005).
2. Eccles JK, Pratson L, Newell RG and Jackson RB, Physical and economic potential of geological CO_2 storage in saline aquifers. *Environ Sci Technol* **43**(6):1962–1969 (2009).
3. Gibbins J and Chalmers H, Carbon capture and storage. *Energy Policy* **36**(12):4317–4322 (2008).
4. Celia MA, Bachu S, Nordbotten JM and Bandilla KW, Status of CO_2 storage in deep saline aquifers with emphasis on modeling approaches and practical simulations. *Water Resour Res* **51**(9):6846–6892 (2015).
5. Freund P and Ormerod WG, Progress toward storage of carbon dioxide. *Energy Convers Manage* **38**:S199-S204 (1997).
6. Bergman PD and Winter EM, Disposal of carbon dioxide in aquifers in the U.S. *Energy Convers Manage* **36**(6):523–526 (1995).
7. Kongsjorden H, Kårstad O and Torp TA, Saline aquifer storage of carbon dioxide in the sleipner project. *Waste Manage* **17**(5):303–308 (1998).
8. Zhang D and Song J, Mechanisms for geological carbon sequestration. *Procedia IUTAM* **10**:319–327 (2014).
9. Bachu S, CO_2 Storage in geological media: role, means, status and barriers to deployment. *Prog Energy Combust Sci* **34**(2):254–273 (2008).
10. Zhao Y, Song Y, Liu Y, Liang H and Dou B, Visualization and measurement of CO_2 flooding in porous media using MRI. *Ind Eng Chem Res* **50**(8):4707–4715 (2011).
11. Vosper H, Kirk K, Rochelle C, Noy D and Chadwick A, Does numerical modelling of the onset of dissolution-convection reliably reproduce this key stabilization process in co_2 storage? *Energy Procedia* **63**:5341–5348 (2014).
12. Mahmoodpour S, Rostami B, Soltanian MR and Amooie MA, Effect of brine composition on the onset of convection during CO_2 dissolution in brine. *Comput Geosci* **124**:1–13 (2019).
13. Thomas C, Dehaeck S and De Wit A, Convective dissolution of CO_2 in water and salt solutions. *Int J Greenhouse Gas Control* **72**:105–116 (2018).
14. Taheri A, Torsæter O, Lindeberg E, Hadia NJ and Wessel-Berg D, Qualitative and quantitative experimental study of convective mixing process during storage of CO_2 in heterogeneous saline aquifers. *Int J Greenhouse Gas Control* **71**:212–226 (2018).
15. Song Y, Nishio M, Chen B, Someya S and Ohsumi T, Measurement on CO_2 solution density by optical technology. *J Visualization* **6**(1):41–51 (2003).
16. Mojtaba S, Behzad R, Rasoul NM and Mohammad R, Experimental study of density-driven convection effects on CO_2 dissolution rate in formation water for geological storage. *J Nat Gas Sci Eng* **21**(Supplement C): 600–607 (2014).
17. Faisal TF, Chevalier S, Bernabe Y, Juanes R and Sassi M, Quantitative and qualitative study of density driven CO_2 mass transfer in a vertical Hele-Shaw cell. *Int J Heat Mass Transfer* **81**(Supplement C):901–914 (2015).
18. Khosrokhavar R, Elsinga G, Farajzadeh R and Bruining H, Visualization and investigation of natural convection flow of CO_2 in aqueous and oleic systems. *J Pet Sci Eng* **122**(Supplement C):230–239 (2014).
19. Neufeld JA, Hesse MA, Riaz A, Hallworth MA, Tchelepi HA and Huppert HE, Convective dissolution of carbon dioxide in saline aquifers. *Geophys Res Lett* **37**(22). (2010). https://doi.org/10.1029/2010GL044728
20. Kneafsey TJ and Pruess K, Laboratory experiments and numerical simulation studies of convectively enhanced carbon

dioxide dissolution. *Energy Procedia* **4**(Supplement C):5114–5121 (2011).

21. Amarasinghe W, Fjelde I, Rydland J-Å and Guo Y, Effects of permeability on CO_2 dissolution and convection at reservoir temperature and pressure conditions: a visualization study. *Int J Greenhouse Gas Control* **99**:103082 (2020).
22. Tang Y, Li Z, Wang R, Cui M, Wang X, Lun Z, *et al*, Experimental study on the density-driven carbon dioxide convective diffusion in formation water at reservoir conditions. *ACS Omega* **4**(6):11082–11092 (2019).
23. Hartline BK and Lister CRB, Thermal convection in a Hele–Shaw cell. *J Fluid Mechanics* **79**(2):379–389 (1977).
24. Bjørlykke K. *Petroleum Geoscience: From Sedimentary Environments to Rock Physics*. Springer, Berlin, Heidelberg. (2015).
25. Satter A and Iqbal GM. Reservoir rock properties, in *Reservoir Engineering*, ed. by Satter A and Iqbal GM. Gulf Professional Publishing, Boston, MA, pp. 29–79. (2016).
26. Jensen JL and Lake LW, The influence of sample size and permeability distribution on heterogeneity measures. *SPE-14901-PA* **3**(02):629–637 (1988).
27. Agartan E, Illangasekare TH, Vargas-Johnson J and Cihan A, Birkholzer J, Experimental investigation of assessment of the contribution of heterogeneous semi-confining shale layers on mixing and trapping of dissolved CO_2 in deep geologic formations. *Int J Greenhouse Gas Control* **93**:102888 (2020).
28. Wang L, Nakanishi Y, Hyodo A and Suekane T, Three-dimensional finger structure of natural convection in homogeneous and heterogeneous porous medium. *Energy Procedia* **114**(Supplement C):5048–5057 (2017).
29. Wang S, Zucheng C, Zhang Y, Jiang L, Liu Y and Yongchen S, Unstable density-driven convection of CO_2 in homogeneous and heterogeneous porous media with implications for deep saline aquifers. *Water Resour Res* (2021). https://doi.org/10.1029/2020WR028132
30. Salibindla AKR, Subedi R, Shen VC, Masuk AUM and Ni R, Dissolution-driven convection in a heterogeneous porous medium. *J Fluid Mechanics* **857**:61–79 (2018).
31. Agartan E, Trevisan L, Cihan A, Birkholzer J, Zhou Q and Illangasekare TH, Experimental study on effects of geologic heterogeneity in enhancing dissolution trapping if supercritical CO_2. *Water Resour Res* **51**(3):1635–1648 (2015).
32. Lassen RN, Plampin M, Sakaki T, Illangasekare TH, Gudbjerg J, Sonnenborg TO, *et al*, Effects of geologic heterogeneity on migration of gaseous CO_2 using laboratory and modeling investigations. *Int J Greenhouse Gas Control* **43**: 213–224 (2015).
33. Teng Y, Jiang L, Fan Y, Liu Y, Wang D, Abudula A, *et al*, Quantifying the dynamic density driven convection in high permeability packed beds. *Magn Reson Imaging* **39**: 168–174 (2017).
34. Trevisan L, Pini R, Cihan A, Birkholzer JT, Zhou Q, González-Nicolás A, *et al*, Imaging and quantification of spreading and trapping of carbon dioxide in saline aquifers using meter-scale laboratory experiments. *Water Resour Res* **53**(1):485–502 (2017).
35. Trevisan L, Pini R, Cihan A, Birkholzer JT, Zhou Q and Illangasekare TH, Experimental analysis of spatial correlation effects on capillary trapping of supercritical CO_2 at the intermediate laboratory scale in heterogeneous porous media. *Water Resour Res* **51**(11):8791–8805 (2015).
36. Lv P, Liu Y, Chen J, Jiang L, Wu B, Liu S, *et al*, Pore-scale investigation of effects of heterogeneity on CO_2 geological storage using stratified sand packs. *Greenhouse Gases: Sci Technol* **7**(6):972–987 (2017).
37. Elenius MT and Gasda SE, convective mixing in formations with horizontal barriers. *Adv Water Resour* **62**:499–510 (2013).
38. Lin C-P, Ni C-F, Lee I-H and Li W-C, Effects of permeability variations on CO_2 convection in anisotropic and heterogeneous saline formations. *Terrest Atmos Oceanic Sci* **27**:121–137 (2016).
39. Rezk MG and Foroozesh J, Study of convective-diffusive flow during CO_2 sequestration in fractured heterogeneous saline aquifers. *J Nat Gas Sci Eng* **69**:102926 (2019).
40. Chen C and Zhang D, Pore-scale simulation of density-driven convection in fractured porous media during geological CO_2 sequestration. *Water Resour Res* **46**(11). (2010). https://doi.org/10.1029/2010WR009453
41. Taheri A, Wessel-Berg D, Torsaeter O and Soroush M. The effects of anisotropy and heterogeneity on CO_2 dissolution in deep saline aquifers. Paper presented at Carbon Management Technology Conference; 2012/1/1/; Orlando, FL. CMTC (2012).
42. Soltanian MR, Amooie MA, Gershenzon N, Dai Z, Ritzi R, Xiong F, *et al*, Dissolution trapping of carbon dioxide in heterogeneous aquifers. *Environ Sci Technol* **51**(13):7732–7741 (2017).
43. Kim M, Kim K-Y, Han WS, Oh J and Park E, Density-driven convection in a fractured porous media: implications for geological CO_2 storage. *Water Resour Res* **55**(7):5852–5870 (2019).
44. Ranganathan P, Farajzadeh R, Bruining H and Zitha PLJ, Numerical simulation of natural convection in heterogeneous porous media for CO_2 geological storage. *Transport in Porous Media* **95**(1):25–54 (2012).
45. Farajzadeh R, Ranganathan P, Zitha PLJ and Bruining J, The effect of heterogeneity on the character of density-driven natural convection of CO_2 overlying a brine layer. *Adv Water Resour* **34**(3):327–339 (2011).
46. Chen C, Zeng L and Shi L, Continuum-scale convective mixing in geological CO_2 sequestration in anisotropic and heterogeneous saline aquifers. *Adv Water Resour* **53**:175–187 (2013).
47. Agartan E, Cihan A, Illangasekare TH, Zhou Q and Birkholzer JT, Mixing and trapping of dissolved CO_2 in deep geologic formations with shale layers. *Adv Water Resour* **105**:67–81 (2017).
48. Cheng P, Bestehorn M and Firoozabadi A, Effect of permeability anisotropy on buoyancy-driven flow for CO_2 sequestration in saline aquifers. *Water Resour Res* **48**(9). (2012). https://doi.org/10.1029/2012WR011939
49. De Meyer T, Hemelsoet K, Van Speybroeck V and De Clerck K, Substituent effects on absorption spectra of ph indicators: an experimental and computational study of sulfonphthaleine dyes. *Dyes Pigm* **102**:241–250 (2014).
50. Thomas C, Lemaigre L, Zalts A, D'Onofrio A and De Wit A, Experimental study of CO_2 convective dissolution: the effect of color indicators. *Int J Greenhouse Gas Control* **42**(Supplement C):525–533 (2015).

51. Héricz D, Sarkadi T, Erdei G, Lazuech T, Lenk S and Koppa P, Simulation of small- and wide-angle scattering properties of glass-bead retroreflectors. *Appl Opt* **56**:3969 (2017).
52. Rueden CT, Schindelin J, Hiner MC, DeZonia BE, Walter AE, Arena ET, *et al*, ImageJ2: ImageJ for the next generation of scientific image data. *BMC Bioinf* **18**(1):529 (2017).
53. Lindeberg E and Wessel-Berg D, Vertical convection in an aquifer column under a gas cap of CO_2. *Energy Convers Manage* **38**:S229—S234 (1997).
54. Flaata AMN. The impact of permeability on density-driven convection during CO2 storage in underground reservoirs. *Master's thesis*. University of Stavanger, Stavanger, Norway. (2019).
55. Gensterblum Y, Ghanizadeh A, Cuss R, Amann A, Krooss B, Clarkson C, *et al*, Gas transport and storage capacity in shale gas reservoirs - a review. part a: transport processes. *J Unconv Oil Gas Resour* **12**: 87–122 (2015).
56. Jørstad A, editor *Johan Sverdrup – Offshore Norway: The Story behind the Giant Sverdrup Discovery*. AAPG International Conference and Exhibition, Singapore (2012).
57. Lindeberg E and Wessel-Berg D, Upscaling studies of diffusion induced convection in homogeneous and heterogeneous aquifers. *Energy Procedia* **4**:3927–3934 (2011).
58. Hebach A, Oberhof A and Dahmen N, Density of water + carbon dioxide at elevated pressures: measurements and correlation. *J Chem Eng Data* **49**(4): 950–953 (2004).
59. Efika EC, Hoballah R, Li X, May EF, Nania M, Sanchez-Vicente Y, *et al*, Saturated phase densities of (CO_2+H_2O) at temperatures from (293 To 450)K and pressures up to 64MPa. *J Chem Thermodyn* **93**: 347–359 (2016).
60. Cadogan SP, Maitland GC and Trusler JPM, Diffusion coefficients of CO_2 and N_2 in water at temperatures between 298.15 K and 423.15 K at pressures up to 45 MPa. *J Chem Eng Data* **59**(2):519–525 (2014).

Widuramina Amarasinghe

Widuramina Amarasinghe is a PhD research fellow at University of Stavanger and employed at NORCE Norwegian Research Centre AS. He has a master's degree in Process Technology and a Bachelor in Chemical and Process Engineering. His PhD work is mainly related to CO_2 storage and he has experience in both CO_2 capture and storage. Widuramina has competence in process development, process simulations, energy and optimization together with various laboratory experience.

Ingebret Fjelde

Ingebret Fjelde is Chief Scientist in the EOR SCAL group at the NORCE Norwegian Research Centre AS. His main research interests are enhanced oil recovery (EOR) methods in sandstone and carbonate rock (wettability alteration, low salinity water flooding, surfactant flooding, CO_2-flooding, new EOR methods, and combination of EOR-methods), formation damage mechanisms and CO_2-storage. Fjelde has authored or co-authored more than 90 papers. He holds an MS degree and a PhD degree in chemistry from the University of Bergen.

Anna Maija Nørstebø Flaata

Anna Maija Nørstebø Flaata has an MSc in petroleum reservoir engineering from the University of Stavanger. She wrote her master thesis about CCS in collaboration with NORCE in 2019. She has been working as an engineer in the oil and gas industry.